Journal of Molecular Structure 1125 (2016) 433–442

Contents lists available at ScienceDirect

Journal of Molecular Structure

journal homepage: http://www.elsevier.com/locate/molstruc

# Molecular structure and computational studies on 2-((2-(4-(3-(2,5-dimethylphenyl)-3-methylcyclobutyl)thiazol-2-yl)hydrazono)methyl) phenol monomer and dimer by DFT calculations

Tuncay Karakurt [a, *], Alaaddin Cukurovali [b], Nuriye Tuna Subasi [c], Ibrahim Kani [d]

[a] Department of Chemical Engineering, Faculty of Engineering and Architecture, Ahi Evran University, 40100, Kırşehir, Turkey
[b] Department of Chemistry, Faculty of Science, Firat University, 23119, Elazig, Turkey
[c] Department of Food Engineering, Faculty of Engineering and Architecture, Ahi Evran University, 40100, Kırşehir, Turkey
[d] Department of Chemistry, Faculty of Science, Anadolu University, 26470, Eskişehir, Turkey

ARTICLE INFO

*Article history:*
Received 10 March 2016
Received in revised form
4 July 2016
Accepted 4 July 2016
Available online 9 July 2016

*Keywords:*
X-ray diffraction
IR and NMR spectroscopy
NLO
AIM
Antitumor agent

ABSTRACT

The title compound, 2-((2-(4-(3-(2,5-Dimethylphenyl)-3-methylcyclobutyl)thiazol-2-yl)hydrazono) methyl)phenol, was characterized by single-crystal X-ray diffraction. In order to calculate molecular geometry along with the infrared, Atoms in Molecules (AIM) analysis and $^{1}H$ and $^{13}C$ NMR chemical shift values, the density functional theory (DFT) method with 6-311G++(d,p) basis set was utilized. Experimental data were then used for comparison. While the title crystal structure is photochromic, the molecule is nonplanar. It takes on an enol form including a forceful intramolecular O–H···N hydrogen bond as well as a forceful intermolecular N–H···N hydrogen bond. The 6-311G++(d,p) basis function was used to examine the intramolecular tautomerism single proton transfer reaction of the hydrogen-bonded enol–imine and keto–amine monomer in the title crystal structure at the B3LYP theory level. Further, the frontier molecular orbitals (FMO), molecular docking and NLO properties were studied by using theoretical calculations. The calculated NLO properties of title compound are much greater than urea. The title compound generates a stable complex with CDK2 as is distinct from the binding energy values. These results proposed that the compound might exhibit inhibitory effect against CDK2. These are important in development of new antitumor agent.



## 1. Introduction

Schiff base containing molecules have been used as starting materials in the synthesis of many drug substances due to their antibacterial, anticancer and antioxidant properties [1]. In general, o-hydroxy Schiff bases which have especially intramolecular N–H···O and O–H···N hydrogen bond and have two different tautomeric structure that referred to as respectively keto-amine and enol-imine have attracted considerable interest.

These compounds have shown photochromism and thermochromism properties. Photochromism feature is available such usage areas as measuring the radiation intensity and control, vision systems and optical computers [2,3]. Thiazole and its derivatives play an important role on anti-inflammatory, analgesic agent on lipoxygenase enzyme activities and inhibitors on biological systems [4,5]. Due to resistance of the bacteria to the drugs used against infectious disease is a real need for new specific antibiotics. Furthermore, these compounds having antifungal effect have been used in drugs to fight harmful fungi and insects in agriculture [6].

Schiff bases compounds have been studied recently due to their potential uses in optical communications many of which display non-linear optic (NLO) behavior [7,8]. NLO materials have become popular in recent years due to their potential applications in optoelectronics, switching, optical communication, computing and dynamic image processing [9,10]. Organic materials show a series of important non–linear optical properties by means of their high molecular hyperpolarizability. NLO materials are classified as multi-level semiconductor structures, molecular based macroscopic assemblies and traditional inorganic solids [11].

Cyclin-dependent kinases are important enzyme group in the cell cycle belonging to the serine/threonine protein kinase group which's activity changing with binding the cyclin partners. In this

* Corresponding author. Tel.: +90 3862803825.
*E-mail address:* tuncaykarakurt@gmail.com (T. Karakurt).

http://dx.doi.org/10.1016/j.molstruc.2016.07.009
0022-2860/

heterodimeric enzyme structure regulate the cell the level of transcription and cell cycle by phosphorylating the substrate to form various stimulating responses [12]. In cancer cells, CDK regulation is seen in problems with the alteration of expression (excess cyclin expression or reduced expression of the inhibitor) of CDKs and their regulators and this event results in excessive cell division [13,14]. CDKs inhibition is seen as a different approach in cancer treatment due to the importance of the regulatory role of CDK in the cell cycle and the transcriptional stage [15,16]. Staurosporine which was used as the first CDK inhibitor can influence a wide range of several kinases [17]. Meijer et al. showed that purines are particularly effective on the CDK, especially CDK2 [18]. Additionally, purine izoesters and biaryl purines were also found to show inhibitory effect [19,20]. After comparing the similarity of the structure of the title compound with the ligands of well-known antitumor targets, trial docking studies suggested that the crystal structure 4LYN of CDK2 (Cyclin-Dependent Kinase 2) as most appropriate target of the title compound.

As biological and NLO effects of light mentioned above, new Schiff base which is a structure of cyclobutane and thiazole derivative was synthesized in an earlier publication [6]. Theoretical IR, NMR spectra, potential energy distribution of the vibration frequency (PED) by using VEDA 4 program [21], frontier molecular orbitals (FMO), the induced dipole moment, polarizability, first hyperpolarizability values were examined in order to support experimental study of the synthesized compound. At the same time the hardness parameters of this energy were studied using with quantum chemical calculations of 6-311G++(d,p) basis set [22] DFT(B3LYP) [23] theory, gaussian09 program [24] and gausview 5 program [25] to examine the graphical gaussian output. In addition, antibacterial and antifungal effect of the synthesized compound has been previously studied experimentally [6], as well as its biological effects were carried out using AutoDock Vina [26] program in theoretically in order to support experimental work. AutoDock tools were used to create docking input files and Discover Studio Visualizer 4.0 software was used to show receptor-ligand interactions.

## 2. The crystal structure determination

X-ray diffraction data of crystals was collected with Bruker AXS APEX CCD [27] diffractometer by using MoKα ray. Structure solution of the crystals was obtained by using direct methods with SHELXT-2014 [28] program. Refinement process was carried out with SHELXL-2014 [29] program which uses full matrix the least squares method to determine the positions of atoms other than hydrogen in solution stage. In the first stage of refinement process isotropic refinement was performed to become more sensitive to the position of the atoms and to determine the missing atom. Refinement result was observed in the absence of missing atoms other than hydrogen and anisotropic refinement was made. At the next stage of refinement hydrogen atoms were determined. Hydrogen atoms' positions were obtained geometrically according to the overlap method. When placing hydrogen atoms geometrically, bond length is fixed as aromatic C–H at 0.93 Å, methylene C–$H_2$ at 0.97 Å, methyl C–$H_3$ at 0.96 Å and N–H at 0.86 Å. After completing the structure solution and refinement process, ORTEP-3 [30] program was used for drawing molecular structure and PLATON [31], WinGX [30] and MERCURY [32] programs were used for calculations.

## 3. Result and discussion

### 3.1. Geometrical structure

Crystal parameters of $C_{23}H_{25}N_3OS$ molecule, data collection and the details of refinement process are given in the Supplementary Material, Table S1, a diagram of the molecule drawn experimentally with 40% probability ellipsoids is given in Fig. 1(a) and input molecule used in Gaussian09 software is given in Fig. 1(b). The synthetic procedure and the experimental spectra ($^1$H NMR and $^{13}$C NMR) are given in the Supplementary Material Section.

The compound has non-planar thiazole, cyclobutane, xylene and phenol ring. Angles between cyclobutane-thiazole and cyclobutane-xylene ring respectively 63.24° and 85.72°. Steric interactions that occur between the side groups on the cyclobutane ring caused a deviation from planarity of these rings. Experimental and calculated bond lengths, bond angles, torsion angles are also shown in the Supplementary Material, Table S2. C1–O1, C7–N1, C11–C13, S1–C10, and C8═N3 experimental bond lengths are 1.372(3), 1.261(3), 1.551(4), 1.718(2) and 1.303(2) Å, respectively and these lengths are in compliance with literature values 1.347(2), 1.263(4), 1.532(3), 1.482(3) and 1.290(3) Å [33,34]. Showing single bond character C1–O1 and double bond character C7═N1 bond lengths support adopting the molecule that form enole-imine. These bond lengths are line with bond length obtained from similar structures enole-imine form [35–37]. Intermolecular N–H···N and intramolecular O–H···N bonds were observed in the title crystal structure. The molecules are attached to each other with these interactions. Molecular structure has adopted the enole-imine form and become stable with O–H···N type intramolecular hydrogen bond. It has been observed that N–H···N hydrogen bonds form $R_2^2(8)$ [38] closed ring according to the symmetry center, in case of O–H···N intramolecular hydrogen bond form S(6) [38] closed ring. N2 atom behaves as a hydrogen bond donor by means of H2A atom to the N3 atom that is located at the (1–x, 1–y, –z).

ORTEP-3 structure which is found at the end of the solution process and packing drawing of the molecule in the unit cell are given in the Supplementary Material, Fig. S1 and Fig. S2, respectively. In further, the data related to hydrogen bonds are given in Table 1.

The coordinates obtained from the X-ray data as the starting geometry were used in theoretical calculation of $C_{23}H_{25}N_3OS$ molecule for monomer (Fig. 1(a)) and dimer (Fig. 1(c)). Geometry optimizations belonged to the system were obtained by using DFT/B3LYP method 6-311G++(d,p) basis set., bond lengths, bond angles were compared with experimental results are listed in Table S2.

### 3.2. Tautomerism

Since tautomerism plays an important role in the determination of molecular properties and their application areas, it has been investigated in detail. With intramolecular proton transfer from oxygen to nitrogen atom tautomerism has happened in the title compound as a result of this proton transfer, two types of tautomeric structures are occurred. These are enol-imine related to O–H···N type hydrogen bonding and keto-amine related to N–H···O hydrogen bonding in the solid state [39]. Some selected structural parameters belonging to the enol-imine, keto-amine and transition state (TS) geometries of the title compound were calculated by using the B3LYP level with 6–311G(d,p) basis set. The calculated imaginary vibrational frequency of the transition state is 953i $cm^{-1}$ for the gas phase. Due to a hydrogen atom migration from atom O1 to N1, several changes occurred in the structure. The distance of atoms N1 and H1 decreases upon the proton transfer enol-imine → TS → keto-amine. Thus it may be inferred that the O1–H1 bond is broken, while a N1–H1 bond (1.348 Å in gas phase) emerges during the intramolecular proton transfer process in the compound [40]. The C7–N1 and C1–O1 bond types indicate tautomeric form. The double bond between the C7 and N1 atoms

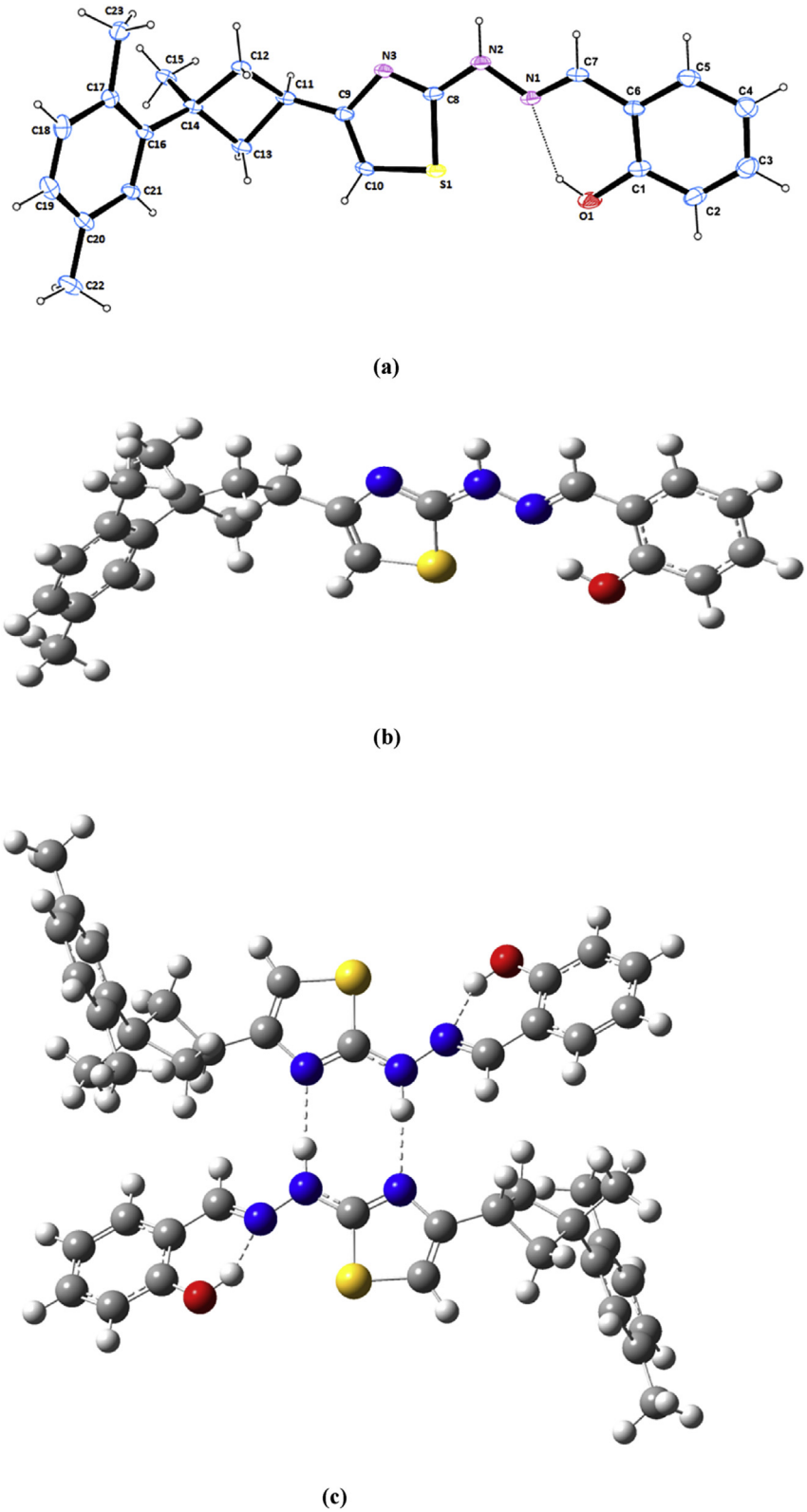


**Fig. 1.** **(a)** ORTEP-3 shape of $C_{23}H_{25}N_3OS$ crystal **(b)** Calculated shape for $C_{23}H_{25}N_3OS$ crystal for monomer structure **c)** for dimer structure.

demonstrate that the title compound was formed as a keto-amine tautomer form. Experimentally, the C7—N1 (1.273 Å) bond owns a double bond character whereas the C1—O1 (1.351 Å) bond owns a single bond character. As can be seen in the Supplementary Material, Fig. S3, O—H···N hydrogen bonding was then formed by O1, H1 and N7 atoms. Ground state energy of the TS, enol-imine and keto-amine were calculated as −4015483.7, −4015540.8 and −4015488.9 kj/mol, respectively. Considering all of these, it seems

**Table 1**
Hydrogen bond geometry for $C_{23}H_{25}N_3OS$ (I) single crystal (Å, °).

| D–H···A | D–H | H···A | D···A | D–H···A |
|---|---|---|---|---|
| N2– H2···N3$^{i}$ | 0.86 (3) | 2.28 (3) | 3.11 (2) | 162 (3) |
| O1– H1···N1 | 0.82 (2) | 1.93 (2) | 2.65 (3) | 146 (2) |

Symmetry codes: i = 1−x,1−y,−z.

that the title compound consists of in enol-imine form in the solid state.

### 3.3. IR spectroscopy

Measured in the range of 4000–400 $cm^{-1}$ IR spectrum and calculated spectra are shown in the Supplementary Material, Fig. S4. Meanwhile, theoretically calculated IR vibration frequency values is given in the Supplementary Material, Table S3. Molecule has 53 atoms, C1 point group symmetry and 153 main vibration frequency. All calculations for vibrational frequencies of monomer and dimer structures were done by using DFT(B3LYP/6-311G++(d,p) basis set. Then, the naming of these vibration modes in detail was made by PED analysis. It is known that DFT calculations were done in gas environment. To match the calculation results with the experimental results for each frequency the value is multiplied by the scalar value of 0.9682 [41]. It was observed that the experimental results were found to be closer to the calculated vibration frequency of dimer structure (Fig. 1(c)). Thus, when experimental and theoretical vibration frequencies are considered together, the proof of existence of the dimer structure in the solid state is proved. Intramolecular or intermolecular non-hydrogen bonding O–H and N–H groups were seen to give free vibration frequency peaks between at 3550–3700 and 3500–3300 $cm^{-1}$, respectively. Frequencies of hydrogen bonding O–H and N–H groups were observed between at 3550–3200 and 3200–2400 $cm^{-1}$ [42,43], respectively. In our study, free vibration frequency of the O–H and N–H groups were observed as 3436 and 3179 $cm^{-1}$ experimentally and these frequencies are indicated respectively as 3422 and 3187 $cm^{-1}$ [44,45] in literature. Theoretically, N–H vibration frequency is calculated as 3101 and 3075 $cm^{-1}$ for the dimer structure, and 3418 $cm^{-1}$ for the monomer structure with 89% PED contribution which is estimated to be pure N–H stretching vibration. Likewise, O–H vibrational frequency for the dimer structure is 3362 $cm^{-1}$ and 3406 $cm^{-1}$ for the monomer structure with 89% PED contribution is estimated to be pure O–H stretching vibration. Molecules in which intramolecular or intermolecular hydrogen bonding in case of N–H or O–H group, are stretched to reduce the bending frequency while increasing the bending vibration frequency values [46]. The bending angle in-plane vibration frequencies of O–H and N–H modes were observed respectively at 1494 $cm^{-1}$ and 1434–1586 $cm^{-1}$ experimentally and these frequencies are indicated at 1392–1491 $cm^{-1}$ [45] and 1637 $cm^{-1}$ [47] in the literature. O–H mode is calculated as 1558/1476 $cm^{-1}$ for the dimer structure, as 1333–1566 $cm^{-1}$ for the monomer structure. N–H mode is calculated as 1582/1611 $cm^{-1}$ for the dimer structure, as 1333–1566 $cm^{-1}$ for the monomer structure. Non-plane angle bending vibration frequency of O–H and N–H modes was experimentally observed respectively at 724 and 636 $cm^{-1}$. These modes are calculated as 723 and 674 $cm^{-1}$ for the dimer structure, 622 and 412 $cm^{-1}$ for the monomer structure. Considering these results it can be concluded that N–H and O–H groups are used for intermolecular bond formation.

C–O group attached to the ring C=N (thiazole) and C=N (hydrazone) vibration frequencies were experimentally observed at 1282, 1618 and 1586 $cm^{-1}$ respectively and these are in compliance with in the literature value [33,48].

Characteristic aromatic compounds' CH vibration frequencies are observed at the range of 3100–3000 $cm^{-1}$ in the IR spectra [49], C–C aromatic stretching vibration generate characteristic band at the range of 1600–1400 $cm^{-1}$ [50]. Aromatic C–H and C–C vibration frequencies found in the two ring were experimentally observed at 3042 and 1618–1434 $cm^{-1}$. Literature values are in compliance with at 3110–3003 and 1666–1535 $cm^{-1}$ [44]. As for the theoretical vibration frequency were calculated in the range of 3096–3049 $cm^{-1}$ for the monomer structure and 3097–3048 $cm^{-1}$ for the dimer structure of molecule. Aromatic CH bending angle in-plane vibration frequency is observed experimentally at 1400–1000 $cm^{-1}$ [51]. Experimentally this vibration frequency was observed at 1148 $cm^{-1}$ and it was calculated in between 1144 and 1098 $cm^{-1}$ for the monomer structure, 1188–1133 $cm^{-1}$ for the dimer structure. It was seen that our experimental measurements and theoretical calculations were in compliance with the literature values [52]. Considering that the molecules have three different $CH_3$ groups, C–H stretching vibrations in the $CH_3$ groups is observed at lower values from those aromatic molecules. Asymmetric C–H stretching vibrations of monomer and dimer structures were calculated as 3000–2972 and 2993–2975 $cm^{-1}$, respectively. They consist of pure C–H modes with the contribution of 35% PED. Similarly, symmetric C–H stretching vibration consists of pure C–H peaks for monomer and dimer structures were calculated as 2738–2924 and 2938–2923 $cm^{-1}$, respectively. As expected, asymmetric vibrations appeared in higher values than the symmetrical vibration values. Most of the hydrocarbons in the $CH_2$ symmetric stretching vibrations emerged at 2900–2850 $cm^{-1}$, asymmetric stretching vibrations are observed at between 3000 and 2900 $cm^{-1}$ [49]. In this study, symmetric $CH_2$ stretching vibration was observed experimentally at 2860 $cm^{-1}$, 2938–2924 $cm^{-1}$ and 2963–2953 $cm^{-1}$ that they were calculated respectively for monomer and dimer structures. Asymmetric $CH_2$ stretching vibrations were calculated for monomer and dimer structures as 2993–2975 $cm^{-1}$ and 3016–3010 $cm^{-1}$, respectively. Other vibration modes are given in Table S3.

### 3.4. NMR spectra

GIAO (Gauge-Independent Atomic Orbital) [53,54] method was used to determine the NMR chemical shift values of molecules and TMS [tetramethylsilane, $Si(CH_3)_4$] was taken as a reference. $^{1}H$ and $^{13}C$ NMR chemical shift values of deuterated chloroform ($CDCl_3$) which was selected for TMS were calculated as 31.30 and 175.58 ppm by using DFT/B3LYP/6-311G++(d,p) basis set. $^{1}H$ and $^{13}C$ NMR chemical shift values of the title compound which were theoretically obtained by using experimentally optimized structures are given in the Supplementary Material, Table S4. When $^{13}C$ NMR spectrum of the molecule is analyzed at the peak of C8 and C9 that is evidence that molecule has thiazole ring. The NMR chemical shift values of these atoms are greater than carbon atoms. Especially, three electronegative atoms (N2, N3 and S1) at around C8 atom due to the high shielding inhibitory effects of these atoms resonates at low field. Because of this reason, chemical shift of C8 atom is measured experimentally at 168.54 ppm which is larger than those of other carbon atoms. C9 atom in the molecule resonate at a higher field and chemical shift of C9 atom is measured experimentally at 154.687 ppm due to less shielding inhibitory effect of the less electronegative C10 and C11 atom with respect to N1 and S1 with N3 atom. In the $^{1}H$ NMR spectrum amine and hydroxy groups of the hydrogen peaks were observed experimentally at 7.28–7.33 and 10.61 ppm, respectively. Theoretical calculations of these peaks have been found 9.22 and 9.60 ppm for the monomer

structure and 11.81 and 9.72 ppm for the dimer structure. Other peaks on the molecule are given in Table S4. Experimental $^{1}H$ and $^{13}C$ NMR spectra of title compound are included as Supplementary Material. (Figs. S5 and S6).

### 3.5. AIM analysis

Bader's QTAIM theory is used for more information about details on the nature and strength of intermolecular and intramolecular hydrogen bonds within the molecule. QTAIM theory is a part of quantum mechanical methods based on the identification of electron density which plays an important role for understanding and explaining the experimental observations of chemistry [55]. Chemical bonding interactions can be characterized and classified by the electron and energy density in the bond critical point (BCP). The strength of the chemical bond is obtained by using electron density in the critical point ($\rho_{BCP}$) [56]. To know the electron density values in the bond critical point ($\rho_{BCP}$) it is almost to know that the bond occurs with what kind of interactions. Laplacian of the electron density of the critical point in BCP is indicated by $\nabla^2(\rho_{BCP})$ and this value is negative in the covalent bonds. For example, for typical C–H bond $\nabla^2(\rho_{BCP}) = -1.1$ au. However, in case of bond formed by ionic, Van der Waals and hydrogen interaction $\nabla^2(\rho_{BCP}) > 0$ due to the reduction in electron density of BCP. For example, for N-(H···O) = C hydrogen bond $\nabla^2(\rho_{BCP}) = +0.03$ a.u. geometric characters can be used to characterize the strength of hydrogen bonds as topological parameters. The presence of hydrogen bonding is supported with some geometrical criteria by Koch and Popelier depending on QTAIM theory as followed: (i) For proton (H)···acceptor (A) the presence of bond critical point is related with a verification of the existence of hydrogen bonding interaction. (ii) The value of the electron density (ρH···A) must be between 0.002 and 0.040 a.u. (iii) $\nabla^2(\rho_{BCP}) =$ value should be between 0.024 and 0.139 a.u. These interactions can be classified as follows by Rozas et al.[57]. (i) Hydrogen bonds with strong covalent character is characterized by $\nabla^2(\rho_{BCP}) < 0$ and $H_{BCP} < 0$ ($H_{BCP}$ which is the total energy density of electrons in the bond critical point). (ii) The moderate hydrogen bonds with partial covalent character is characterized by $\nabla^2(\rho_{BCP}) > 0$ and $H_{BCP} < 0$. (iii) Weak hydrogen bonds which have electrostatic character are characterized by $\nabla^2(\rho_{BCP}) > 0$ and $H_{BCP} > 0$ and the distance between the interacting atoms is greater than Van der Waals Radius. Molecular graph of dimer structure is shown in Fig. 2 by using AIMAll program [58].

The geometrical parameters of intramolecular and intermolecular interaction and the sum of the Van der Waal's Radius of interacting atoms are given in Table 2.

Parameters such as bond angle (D–H···A) and distance between the interacting atoms (H···A) are in compliance with hydrogen bonding criteria for N–H···N and O–H···N interactions while the C–H···C interaction is not. Topological parameters for interacting atoms bond in the bond critical point (BCP) are given in Table 3. Laplacian electron density value of C12–H12···C7 hydrogen bonding interaction is not compatible with Koch and Popelier criteria where it is deviated from hydrogen bond category. Various types of observed interactions on molecular graphics are classified depending on geometrical, topological and energetic parameters. Also Bader's theory was used to calculate the hydrogen bond energy in this study. Espinosa proposed the relationship between hydrogen bond interactions energy with potential energy density as $E_{int} = 1/2(V_{BCP})$ [59]. According to interaction energy ($E_{int}$), the strength of the interaction is given as the following. As can be seen N–H···N hydrogen bond interaction is stronger than O–H···N hydrogen bond interactions. In addition, according to AIM calculations the total binding energy of dimer structure was calculated as 11.6 kcal/mol.

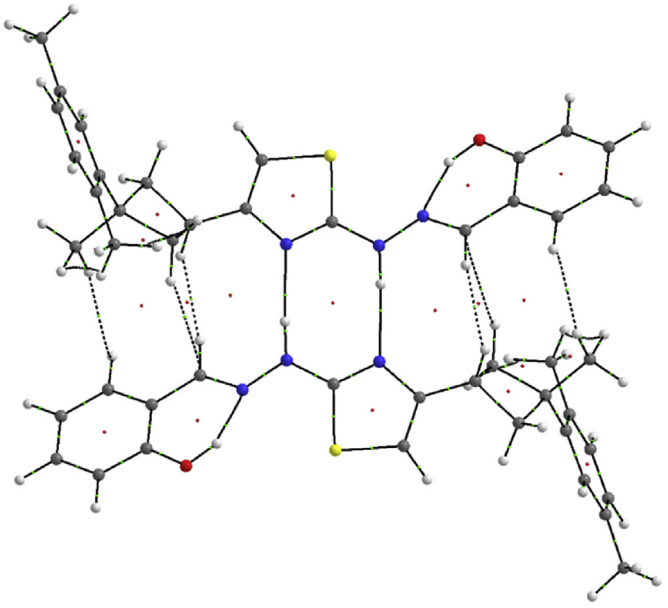

**Fig. 2.** Molecular graph of dimer: bond critical points (small red spheres), ring critical points (small yellow sphere), bond paths (pink lines). (For interpretation of the references to color in this figure legend, the reader is referred to the web version of this article.)

**Table 2**
Geometrical parameters for intra and intermolecular interactions: bond distance (Å), bond angle (°) and sum of van der Wall's radii of interacting atoms (rH + rA) in Å.

| Interaction | D–H | H···A | D···A | D–H···A | ($r_H + r_A$) |
|---|---|---|---|---|---|
| N60–H61···N13 | 1.03 | 2.02 | 3.04 | 171.41 | 2.75 |
| N17–H18···N56 | 1.03 | 2.02 | 3.04 | 171.41 | 2.75 |
| O69–H70···N64 | 0.98 | 1.82 | 2.68 | 144.42 | 2.75 |
| O26–H27···N21 | 0.98 | 1.82 | 2.68 | 144.42 | 2.75 |
| C9–H35···C62 | 1.09 | 3.00 | 3.81 | 131.29 | 2.90 |
| C52–H78···C19 | 1.09 | 3.00 | 3.81 | 131.29 | 2.90 |

### 3.6. Frontier molecular orbitals and molecular hardness

After obtaining stable structures and structural parameters, induced dipole moment, polarizability, hyperpolarizability, the HOMO and LUMO energy values were examined. At the same time the hardness of the molecule is obtained from the energy. The effect of different electron realizing group on these properties was investigated.

The most important orbitals in a molecule are frontier molecular orbitals called HOMO and LUMO. These orbitals describe intramolecular interactions. HOMO energy indicates the tendency to receive electrons. The energy difference between the two orbitals is a measure of chemical stability and a critical parameter in determining the molecular electrical transport properties since it is a measure of electron conductivity. Therefore, this energy difference is largely responsible for chemical and spectroscopic properties of molecules [60]. Calculations have been carried out in the gas phase, molecules HOMO (Fig. 3(a)) and LUMO (Fig. 3(b)) energy values are calculated as −5.57 and 1.74 eV and 3.83 eV for the difference between these energy levels (($\Delta E_{HOMO\text{-}LUMO}$). As shown in Fig. 3(a), the electron donating phenol, thiazole and amine groups are localized the HOMO orbitals in the title molecule.

Electronic molecular features such as electron density and frontier molecular orbital density fields (HOMO and LUMO) are important concept to explain biological activity and molecular properties. When the ligands having functionally much electron

**Table 3**
Topological parameters for bonds of interacting atoms: electron density ($\rho_{BCP}$), Laplacian of electron density ($\nabla^2\boldsymbol{\rho_{BCP}}$), kinetic electron energy density ($G_{BCP}$), potential electron energy density ($V_{BCP}$), total electron energy density ($H_{BCP}$), estimated interaction energy ($E_{int}$) at bond critical point (BCP).

| Interaction | $\rho_{BCP}$ (a.u.) | $\nabla^2\boldsymbol{\rho_{BCP}}$ (a.u.) | $G_{BCP}$ (a.u.) | $V_{BCP}$ (a.u.) | $H_{BCP}$ (a.u.) | $E_{int}$ (kcal/mol) |
|---|---|---|---|---|---|---|
| H61···N13 | 0.0264 | 0.0733 | 0.0175 | −0.0166 | 0.0009 | −5.208333 |
| H18···N56 | 0.0264 | 0.0733 | 0.0175 | −0.0166 | 0.0009 | −5.208333 |
| H70···N64 | 0.0397 | 0.1103 | 0.0309 | −0.0342 | −0.0033 | −10.730421 |
| H27···N21 | 0.0397 | 0.1103 | 0.0309 | −0.0342 | −0.0033 | −10.730421 |
| H35···C62 | 0.042 | 0.0131 | 0.0026 | −0.0019 | 0.0007 | −0.5961345 |
| H78···C19 | 0.0042 | 0.0131 | 0.0026 | −0.0019 | 0.0007 | −0.5961345 |

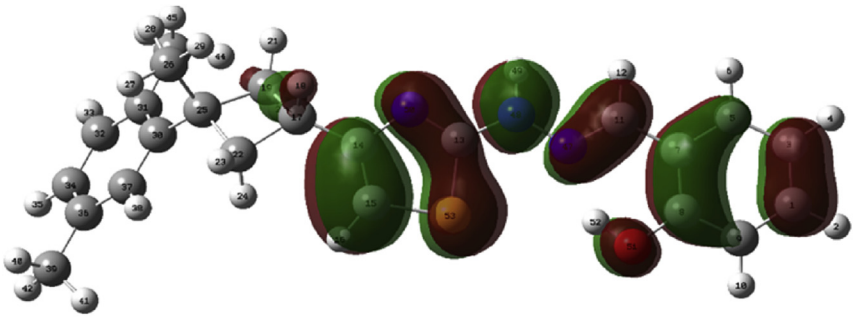

**(a)**

**HOMO (-5.57 eV)**

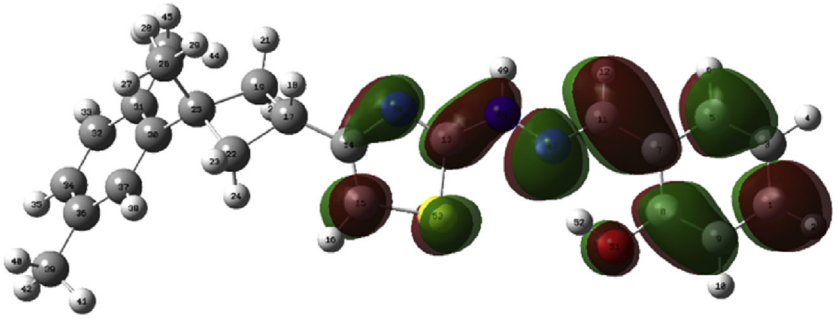

**(b)**

**LUMO (-1.74 eV)**

**Fig. 3.** Molecular orbital surfaces and energy levels given in parentheses for the HOMO and LUMO.

transferring capacity they can donate the electrons to the proteins in order to be better interactions. Molecular mechanism of ligand-binding site was explained at the quantum chemical level as follows: the highest occupied molecular orbital (HOMO) on the nucleophilic molecule (drug) interacts with the lowest unoccupied molecular orbital (LUMO) on the electrophilic agent (enzyme active site) [61].

Molecular hardness parameters are obtained from the finite difference formula which is suggested by parr and Pearson [62] and hardness parameters were calculated using the operational definition of $\eta$ [63]:

$$\eta = 1/2\ (IE - EA)$$

Here IE shows the first ionization energy and EA shows the electron affinity. This situation is known as the Koopman theorem. Hardness value can provide the following approach through the highest occupied molecular orbital energy ($E_{HOMO}$) and the lowest unoccupied molecular orbital energy ($E_{LUMO}$):

$$\eta \approx 1/2(E_{LUMO} - E_{HOMO})$$

Some studies in the literature examined the effect of hardness parameters $\eta$ on the charge transfer and it is stated that small $\eta$ value correspond to a more powerful charge transfer [64–66] in this study. Hardness value was calculated as 1.92. Calculated hardness value of molecule is smaller than in literature value of 2.04 [45], 2.05 [67]. This situation shows that the charge transfer will be stronger in the molecule.

### 3.7. Non-linear optical property

In this section non-linear optical properties of the molecule were investigated by B3LYP/6-311++G(d) method. Organic materials that light waves can interact in exhibit non-linear optical property are used for optical storage applications with fast data

access [68]. These optical properties are determined by the polarizability. The polarizability of a molecule is defined as shown in the linear response to the electric field which is applied to the dipole moment [69]. If polarizability depends on the direction of the applied field, it is called anisotropic. If it is independent of the direction of the applied field, it is called isotropic polarizability. Taking cartesian coordinates into consideration, the relationship between electronic dipole moment $\{\mu_i(i = x, y, z)\}$ a molecule and total dipole moment $(\mu_{tot})$ is given as follows:

$$\mu_{tot} = \left(\mu_x^2 + \mu_y^2 + \mu_z^2\right)^{1/2}$$

According to the calculation performed average polarizability $\alpha_{tot}$ and anisotropic polarizability $\Delta\alpha$ is calculated by the following statements [70].

$$\alpha_{tot} = \frac{1}{3}\left(\alpha_{xx} + \alpha_{yy} + \alpha_{zz}\right)$$

$$\Delta\alpha = \frac{1}{\sqrt{2}}\Big[\left(\alpha_{xx} - \alpha_{yy}\right)^2 + \left(\alpha_{yy} - \alpha_{zz}\right)^2 + \left(\alpha_{zz} - \alpha_{xx}\right)^2 + 6\alpha_{xz}^2 + 6\alpha_{xy}^2 + 6\alpha_{yz}^2\Big]^{1/2}$$

Here, $\alpha_{xx}, \alpha_{xy}, \alpha_{yy}, \alpha_{xz}, \alpha_{yz}, \alpha_{zz}$ are polarizability tensors and they are obtained from the output files of vibration frequency calculations which are performed theoretically by Gaussian09 program.

First hyperpolarizability of a molecule is a measure against this non-linear response of the electric field that is applied to an electric field of the dipole moment of the molecule. The way to increase the non-linear optical properties of the molecules which increases the length of the molecule with conjugated π bonds or donor-acceptor group is binding to the molecular ands. In a system where electron acceptor-donor groups are connected polarizability and the first hyperpolarizability values depend on the electronic Exchange between the electron acceptor and donor groups and that plays a key role in the intramolecular charge transfer [71]. Therefore, hyperpolarizability is observed due to the degeneracy of the local charge distribution on the molecule by π-electron density usually in an electron acceptor-donor groups connected system. In the presence of an applied external field the energy of the system is a function of electric field. Molecules which have high first hyperpolarizability value are called second order NLO materials and said feature has a very important place in technological applications. If the external field is applied to a molecule, dipole moment response is nonlinear and this response is called the hyperpolarizability. Accordingly, the first hyperpolarizability value:

$$\langle\beta\rangle = \left[\left(\beta_{xxx} + \beta_{xyy} + \beta_{xzz}\right)^2 + \left(\beta_{yyy} + \beta_{yzz} + \beta_{yxx}\right)^2 + \left(\beta_{zzz} + \beta_{zxx} + \beta_{zyy}\right)^2\right]^{1/2}$$

is calculated by this statement [9,72–74] and here

$$\beta_x = \left(\beta_{xxx} + \beta_{xyy} + \beta_{xzz}\right)$$

$$\beta_x = \left(\beta_{yyy} + \beta_{yzz} + \beta_{yxx}\right)$$

$$\beta_x = \left(\beta_{zzz} + \beta_{zxx} + \beta_{zyy}\right)$$

Is defined. As in the polarizability tensors fist hyperpolarizability is obtained from the result of frequency calculations of $\beta_{xxx}, \beta_{xxy}, \beta_{xyy}, \beta_{yyy}, \beta_{xxz}, \beta_{xyz}, \beta_{yyz}, \beta_{xzz}, \beta_{yzz}, \beta_{zzz}$ . The first hyperpolarizability vector component is calculated as follows [9]:

$$\beta_{vec} = \sum_{i=1}^{3} \frac{\mu_i\beta_i}{|\mu|}$$

In this formula $|\mu|$ is ground state molecular electronic dipole moment and $\mu_i$ is the vector component of the dipole moment in question. $\beta_i$ is represented by $\beta_x$, $\beta_y$, $\beta_z$.

Calculated values are converted into electrostatic unit (esu) (for α; 1 a.u. = $0.1482 \times 10^{-24}$ esu, for β; 1 a.u. = $8.6393 \times 10^{-33}$ esu).

For molecules examined in this study, the polarizability tensor components, the average polarizability ($\alpha_{tot}$), anisotropic polarizability ($\Delta\alpha$), the first hyperpolarizability tensor components, the first hyperpolarizability ($\langle\beta\rangle$) and the vector component ($\beta_{vec}$) are given in atomic and electronic unit in the Supplementary Material, Table S5.

The dipole moment value which plays a very important role in the nonlinear effects is calculated as 2.20D. This value indicates that positive and negative charge centers arranged quite far from each other. This means that deterioration of local charge distribution in the molecule cause charge polarization. In addition to the biggest dipole moment component for the molecule was obtained in the y direction and is calculated as a positive value given to the z direction of component for molecules. Arrangement of the investigated molecules in x, y, z cartesian coordinate and orientation of dipole moment are shown in Fig. 4.

Calculated polarizability and first hyperpolarizability tensors give different values from zero for all directions. This indicates that investigated molecules are NLO active. In studies to determine the NLO properties of molecular systems, the comparison is made with crystalline urea which known as a good NLO active molecule. According to the calculations made in this study $\alpha_{tot}$ and $\beta_{tot}$ values were found respectively as 52.52 $Å^3$ and $22.95 \times 10^{-30}$ $cm^5$/esu. It is emerged that investigated title molecule has 30 times greater value than the first hyperpolarizability value of urea ($\alpha_{tot}$ and $\beta_{tot}$ values for urea were calculated as 4.91 $Å^3$ and $0.79 \times 10^{-30}$ $cm^5$/esu with (B3LYP/6-311G++(d,p)). Compared to previously-worked Schiff base-like molecules in the literature $\beta_{tot}$ value of the molecule studied in this work that it was calculated greater than $3.946 \times 10^{-30}$ $cm^5$/esu [75] and $19.33 \times 10^{-30}$ [76] $cm^5$/esu is observed. As we know that a small energy gap between HOMO and LUMO cause to high polarizability on the other hand large energy gap between HOMO and LUMO cause low polarizability. This correlation of the inverse relationship was reported previously[77]. These result demonstrated that the title compound is preferred as a good NLO material.

### 3.8. Molecular docking studies

CDK2 (Cyclin-Dependent Kinase 2) crystal structure (pdb code: 4LYN) for docking study is provided through the Protein Data Bank (http://www.rcsb.org/pdb). Before the docking process water molecules were removed from 4LYN structure, hydrogen atoms and Gasteiger charges were added to 4LYN structure. After this process, docking (Fig. 5(a)) is made to binding site of the target molecule with used ligand. Estimated binding energy (docking score) and RMSD values were obtained from molecular docking results and numerical results are shown comparatively in Table 4.

When the RMSD value of the obtained docking results is smaller than 2 Å, it is specified as correct [78]. RMSD value is the root mean square deviation from the determined conformation of the ligand structure. In other words, it means that the deviation from the

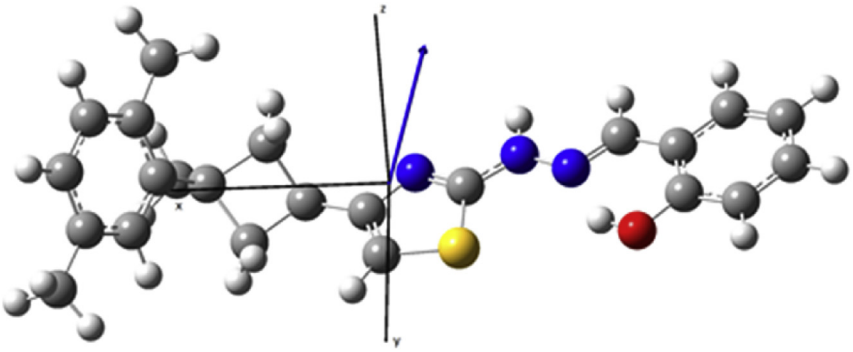

**Fig. 4.** Cartesian coordinates and dipole moment (blue arrow) of the molecule. (For interpretation of the references to colour in this figure legend, the reader is referred to the web version of this article.)

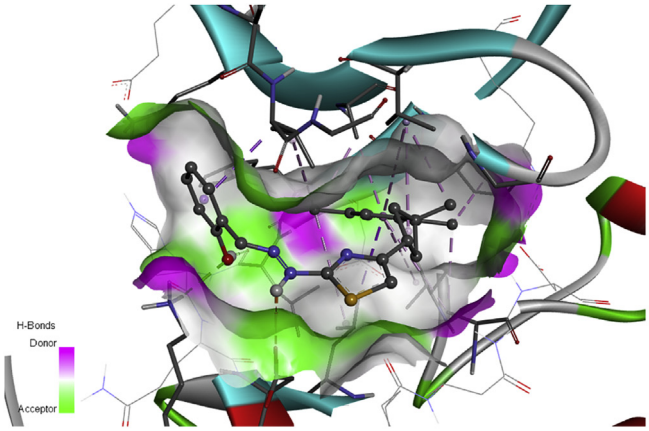


(a)

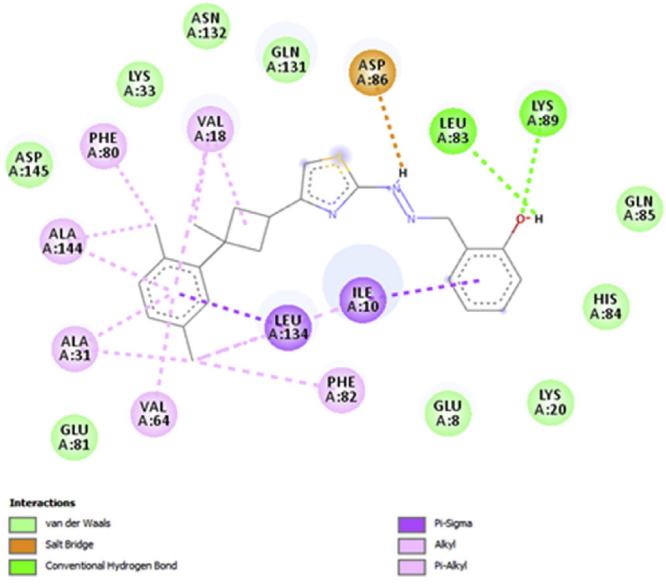


(b)

**Fig. 5.** (a) Docking result of molecule representation (b) Ligand interaction diagrams of receptor ligand complexes. H-bond, π-π and π-alkyl interactions is shown respectively as green, pink and orange lines. (For interpretation of the references to colour in this figure legend, the reader is referred to the web version of this article.)

**Table 4**
Affinity and RMS values belonging to different conformations of the molecule.

| Mode | Affinity (kcal/mol) | Distance from best mode | |
|---|---|---|---|
| | | RMSD 1.b. | RMSD u.b. |
| 1 | −10.3 | 0.000 | 0.000 |
| 2 | −9.8 | 2.944 | 6.674 |
| 3 | −9.7 | 1.618 | 2.689 |
| 4 | −9.3 | 4.346 | 7.746 |
| 5 | −9.3 | 5.691 | 9.168 |
| 6 | −9.2 | 1.511 | 2.019 |
| 7 | −9.1 | 2.772 | 6.681 |
| 8 | −9.1 | 3.348 | 4.868 |
| 9 | −9.0 | 2.821 | 7.275 |

active site where the ligand interact is the most important criteria for the docking results. The binding energy is the criterion which was looked after the RMSD value.

The reason of this priority is that the structure could also give lower binding energy with a place other than the active site so first its proximity to the active site is looked at and then its binding energy of the active region.

It was observed that ligand is bound to the substrate binding region of receptors with weak non-covalent interactions. More specifically it is bonded to with hydrogen bonding, π-sigma and π-π-alkyl interactions. As seen in Fig. 5(b) between LYS89 and LUE83 with oxygen atom of ligand hydrogen bonds were formed 2.503 and 2.728 Å in length. As shown in Fig. 5(b), ILE10 is bound to phenol ring of ligand with π-sigma interaction, LEU134 with π-sigma interaction ALA144, ALA31, VAL64 and VAL18 are bonded to xylene ring with π-alkyl interactions, VAL18 is bound to cyclobutane ring with π-alkyl interactions and PHE80, ALA144, ALA31 and PHE82 are bound to ligand with alkyl-alkyl interactions.

According to the calculated binding affinity of ligand, CDK2 is determined as an inhibitor candidate molecule for target structure. All of these showed that this ligand can be selected as a candidate of potential inhibitor compound for designing a drug which has big selectivity.

## 4. Conclusions

In this study, 2-((2-(4-(3-(2,5-Dimethylphenyl)-3-methylcyclobutyl)thiazol-2-yl)hydrazono)methyl)phenol structure that have been synthesized in the previous study is clarified by x-ray diffraction and IR, NMR spectroscopic methods. Also, the molecular structure of title molecule, IR and NMR spectra were

determined and performed by the comparisons with obtained results by experimentally. After stable structures have been calculated and structural parameters of the compound induced dipole moment, polarizability, hyperpolarizability, HOMO, LUMO energies, the hardness parameters were obtained from this energy. In this study hardness value of title compound was smaller than the literature value and this showed that a stronger intramolecular charge transfer. At the same time, the hyperpolarizability value of the molecule was observed higher than the literature values and this showed that the molecule could be preferred as NLO material. Finally, docking simulation was applied to obtain the possible bonding patterns and conformations for the title molecule. The obtained results showed that this compound will be a new potential candidate inhibitor compound.

## Acknowledgement

This study was supported financially by the Research Centre of Ahi Evran University (PYO-FEN.4001.13.011). In addition, computing resources used in this work were provided by the National Center for High Performance Computing of Turkey (UHeM) under grant number 1002742013.

## Appendix A. Supplementary data

Supplementary data related to this article can be found at http://dx.doi.org/10.1016/j.molstruc.2016.07.009.

## References

[1] D.R. Williams, Metals, ligands, and cancer, Chem. Rev. 72 (1972) 203–213.
[2] H. Dürr, Perspectives in photochromism: a novel system based on the 1, 5-electrocyclization of heteroanalogous pentadienyl anions, Angew. Chemie Int. Ed. Engl. 28 (1989) 413–431.
[3] H. Dürr, H. Bouas-Laurent, Photochromism: Molecules and Systems: Molecules and Systems, Gulf Professional Publishing, 2003.
[4] D. Hadjipavlou-Litina, A. Geronikaki, Anti-inflammatory activity of some novel 1-[3-(aroylo)] and one 1-[3-(aryloxy)]-propyl aminothiazole in correlation with structure and lipophilicity, Arzneimittel-Forschung 46 (1996) 805–808.
[5] B.S. Holla, K. Malini, B.S. Rao, B. Sarojini, N.S. Kumari, Synthesis of some new 2, 4-disubstituted thiazoles as possible antibacterial and anti-inflammatory agents, Eur. J. Med. Chem. 38 (2003) 313–318.
[6] A. Cukurovali, I. Yilmaz, S. Gur, C. Kazaz, Synthesis, antibacterial and antifungal activity of some new thiazolylhydrazone derivatives containing 3-substituted cyclobutane ring, Eur. J. Med. Chem. 41 (2006) 201–207.
[7] M. Jalali-Heravi, A. Khandar, I. Sheikshoaie, A theoretical investigation of the structure, electronic properties and second-order nonlinearity of some azo Schiff base ligands and their monoanions, Spectrochim. Acta Part A Mol. Biomol. Spectrosc. 55 (1999) 2537–2544.
[8] M. Jalali-Heravi, A. Khandar, I. Sheikshoaie, Characterisation and theoretical investigation of the electronic properties and second-order nonlinearity of some three dentate salicylaldiminato Schiff base ligands, Spectrochim. Acta Part A Mol. Biomol. Spectrosc. 56 (2000) 1575–1581.
[9] D.R. Kanis, M.A. Ratner, T.J. Marks, Design and construction of molecular assemblies with large second-order optical nonlinearities. Quantum chemical aspects, Chem. Rev. 94 (1994) 195–242.
[10] P.N. Prasad, D.J. Williams, Introduction to Nonlinear Optical Effects in Molecules and Polymers, Wiley New York etc, 1991.
[11] D. Avcı, A. Başoğlu, Y. Atalay, Ab initio HF and DFT calculations on an organic non-linear optical material, Struct. Chem. 21 (2010) 213–219.
[12] M. Malumbres, M. Barbacid, Mammalian cyclin-dependent kinases, Trends Biochem. Sci. 30 (2005) 630–641.
[13] M. Hall, G. Peters, Genetic alterations of cyclins, cyclin-dependent kinases, and Cdk inhibitors in human cancer, Adv. Cancer Res. 68 (1996) 67–108.
[14] C.J. Sherr, Cancer cell cycles, Science 274 (1996) 1672–1677.
[15] I. Collins, M.D. Garrett, Targeting the cell division cycle in cancer: CDK and cell cycle checkpoint kinase inhibitors, Curr. Opin. Pharmacol. 5 (2005) 366–373.
[16] G.I. Shapiro, Cyclin-dependent kinase pathways as targets for cancer treatment, J. Clin. Oncol. 24 (2006) 1770–1783.
[17] A.M. Lawrie, M. Noble, P. Tunnah, N.R. Brown, L.N. Johnson, J.A. Endicott, Protein kinase inhibition by staurosporine revealed in details of the molecular interaction with CDK2, Nat. Struct. Biol. 4 (1997) 796–801.
[18] K. Brachwitz, B. Voigt, L. Meijer, O. Lozach, C. Schächtele, J. Molnár, A. Hilgeroth, Evaluation of the first cytostatically active 1-aza-9-oxafluorenes as novel selective CDK1 inhibitors with P-glycoprotein modulating properties, J. Med. Chem. 46 (2003) 876–879.
[19] F. Popowycz, G. Fournet, C. Schneider, K. Bettayeb, Y. Ferandin, C. Lamigeon, O.M. Tirado, S. Mateo-Lozano, V. Notario, P. Colas, Pyrazolo [1, 5-a]-1, 3, 5-triazine as a purine bioisostere: access to potent cyclin-dependent kinase inhibitor (R)-roscovitine analogue, J. Med. Chem. 52 (2009) 655–663.
[20] M.P. Trova, K.D. Barnes, C. Barford, T. Benanti, M. Bielaska, L. Burry, J.M. Lehman, C. Murphy, H. O'Grady, D. Peace, Biaryl purine derivatives as potent antiproliferative agents: inhibitors of cyclin dependent kinases. Part I, Bioorg. Med. Chem. Lett. 19 (2009) 6608–6612.
[21] M.H. Jamroz, Vibrational energy distribution analysis (VEDA): scopes and limitations, Spectrochim. Acta A Mol. Biomol. Spectrosc. 114 (2013) 220–230.
[22] G. Rauhut, S. Puyear, K. Wolinski, P. Pulay, Comparison of NMR shieldings calculated from Hartree-Fock and density functional wave functions using gauge-including atomic orbitals, J. Phys. Chem. 100 (1996) 6310–6316.
[23] R. Ditchfield, W.J. Hehre, J.A. Pople, Self-consistent molecular-orbital methods. IX. An extended Gaussian-type basis for molecular-orbital studies of organic molecules, J. Chem. Phys. 54 (1971) 724–728.
[24] M. Frisch, G. Trucks, H.B. Schlegel, G. Scuseria, M. Robb, J. Cheeseman, G. Scalmani, V. Barone, B. Mennucci, G. Petersson, Gaussian 09, Revision A. 02, vol. 19, Gaussian, Inc, Wallingford, CT, 2009, pp. 227–238.
[25] R. Dennington, T. Keith, J. Millam, GaussView, Version 5, Semichem Inc., Shawnee Mission, KS, 2009.
[26] O. Trott, A.J. Olson, AutoDock Vina: improving the speed and accuracy of docking with a new scoring function, efficient optimization, and multithreading, J. Comput. Chem. 31 (2010) 455–461.
[27] A.V. Bruker, 1 and SAINT Version 7.34 a Data Collection and Processing Software, Bruker Analytical X-Ray Instruments, Inc., Madison, WI, USA, 2009.
[28] G.M. Sheldrick, SHELXT – Integrated space-group and crystal-structure determination, Acta. Cryst. Sect. A Found. Adv. 71 (2015) 3–8.
[29] G.M. Sheldrick, Crystal structure refinement with SHELXL, Acta Crystallogr. Sect. C. Struct. Chem. 71 (2015) 3–8.
[30] L.J. Farrugia, WinGX and ORTEP for Windows: an update, J. Appl. Crystallogr. 45 (2012) 849–854.
[31] A.L. Spek, PLATON SQUEEZE: a tool for the calculation of the disordered solvent contribution to the calculated structure factors, Acta Crystallogr. Sect. C. Struct. Chem. 71 (2015) 9–18.
[32] C.F. Macrae, I.J. Bruno, J.A. Chisholm, P.R. Edgington, P. McCabe, E. Pidcock, L. Rodriguez-Monge, R. Taylor, J.v. Streek, P.A. Wood, Mercury CSD 2.0–new features for the visualization and investigation of crystal structures, J. Appl. Crystallogr. 41 (2008) 466–470.
[33] N. Özdemir, M. Dinçer, A. Çukurovalı, An experimental and theoretical approach to the molecular structure of 2-{4-[3-(2, 5-dimethylphenyl)-3-methylcyclobutyl] thiazol-2-yl} isoindoline-1, 3-dione, J. Mol. Model. 16 (2010) 291–302.
[34] H. Ünver, A. Karakas, A. Elmali, Nonlinear optical properties, spectroscopic studies and structure of 2-hydroxy-3-methoxy-N-(2-chloro-benzyl)-benzaldehyde-imine, J. Mol. Struct. 702 (2004) 49–54.
[35] D. Dey, S. Dey, A. Elmali, Y. Elerman, Molecular structure and conformation of N-2-[3′-(methoxysalicylideneimino) benzyl]-3″-methoxysalicylideneimine, J. Mol. Struct. 562 (2001) 177–184.
[36] M. Kabak, A. Elmali, Y. Elerman, T. Durlu, Conformational study and structure of bis-N, N′-p-bromo-salicylideneamine-1, 2-diaminobenzene, J. Mol. Struct. 553 (2000) 187–192.
[37] H. Ünver, A. Karakaş, A. Elmali, T. Durlu, The investigation of nonlinear optical properties of N-(3-fluorophenyl) naphthaldimine, J. Mol. Struct. 737 (2005) 131–137.
[38] M.C. Etter, Encoding and decoding hydrogen-bond patterns of organic compounds, Acc. Chem. Res. 23 (1990) 120–126.
[39] Ö Tamer, D. Avcı, Y. Atalay, Quantum chemical characterization of N-(2-hydroxybenzylidene) acetohydrazide (HBAH): a detailed vibrational and NLO analysis, Spectrochim. Acta Part A Mol. Biomol. Spectrosc. 117 (2014) 78–86.
[40] N. Özdemir, Quantum chemical investigation of the intra-and intermolecular proton transfer reactions and hydrogen bonding interactions in 4-amino-5-(2-hydroxyphenyl)-2H-1, 2, 4-triazole-3 (4H)-thione, J. Mol. Model. 19 (2013) 397–406.
[41] J.P. Merrick, D. Moran, L. Radom, An evaluation of harmonic vibrational frequency scale factors, J. Phys. Chem. A 111 (2007) 11683–11700.
[42] H.A. Dabbagh, A. Teimouri, A.N. Chermahini, M. Shahraki, DFT and ab initio study of structure of dyes derived from 2-hydroxy and 2, 4-dihydroxy benzoic acids, Spectrochim. Acta Part A Mol. Biomol. Spectrosc. 69 (2008) 449–459.
[43] D.M. Smith, Dihydrobenzimidazoles, benzimidazolones, benzimidazolethiones, and related compounds, in: Chemistry of Heterocyclic Compounds: Benzimidazoles and Cogeneric Tricyclic Compounds, Part 1, vol. 40, 1981, pp. 331–389.
[44] D. Avcı, Y. Atalay, M. Şekerci, M. Dinçer, Molecular structure and vibrational and chemical shift assignments of 3-(2-Hydroxyphenyl)-4-phenyl-1H-1, 2, 4-triazole-5-(4H)-thione by DFT and ab initio HF calculations, Spectrochim. Acta Part A Mol. Biomol. Spectrosc. 73 (2009) 212–217.
[45] H. Tanak, Crystal structure, spectroscopy, and quantum chemical studies of (E)-2-[(2-Chlorophenyl) iminomethyl]-4-trifluoromethoxyphenol, J. Phys. Chem. A 115 (2011) 13865–13876.
[46] Ç. Yüksektepe, N. Çalişkan, I. Yilmaz, A. Cukurovali, synthesis, crystal structure, spectroscopic and electronic properties of (E)-Trans-2-(2-(biphenyl-4-ylmethylene) Hydrazinyl)-4-(3-methyl-3-phenylcyclobutyl) thiazole,

J. Chem. Crystallogr. 40 (2010) 1049–1059.
[47] Ö. Tamer, N. Dege, G. Demirtaş, D. Avcı, Y. Atalay, M. Macit, A.A. Ağar, An experimental and theoretical study on the novel (Z)-1-((naphthalen-2-ylamino) methylene) naphthalen-2 (1H)-one crystal, Spectrochim. Acta Part A Mol. Biomol. Spectrosc. 117 (2014) 13–23.
[48] N. Özdemir, E. İnkaya, E. Sarıpınar, L. Akyüz, İ.Ö. İlhan, S. Aydın, M. Dinçer, O. Büyükgüngör, Synthesis, spectroscopic (FT-IR/NMR) characterization, X-ray structure and DFT studies on (E)-2-(1-phenylethylidene) hydrazinecarboximidamide nitrate hemimethanol, Spectrochim. Acta Part A Mol. Biomol. Spectrosc. 114 (2013) 175–182.
[49] G. Varsányi, Assignments for Vibrational Spectra of Seven Hundred Benzene Derivatives, Halsted Press, 1974.
[50] K. Furić, V. Mohaček, M. Bonifačić, I. Štefanić, Raman spectroscopic study of $H_2O$ and $D_2O$ water solutions of glycine, J. Mol. Struct. 267 (1992) 39–44.
[51] J. Mohan, Organic Spectroscopy: Principles and Applications, CRC Press, 2004.
[52] G. Camı, E. Chufán, J. Pedregosa, E. Varetti, Infrared and Raman spectra of 5-amino-1, 3, 4-thiadiazole-2-sulfonamide (Hats). Experimental data and quantum chemistry calculations, J. Mol. Struct. 570 (2001) 119–127.
[53] R. Ditchfield, Molecular orbital theory of magnetic shielding and magnetic susceptibility, J. Chem. Phys. 56 (1972) 5688–5691.
[54] P. Pulay, K. Wolinski, J. Hinton, The 3–21+ G basis set for first row elements, J. Am. Chem. Soc. 112 (1990) 8251–8260.
[55] A. Becke, C.F. Matta, R.J. Boyd, The Quantum Theory of Atoms in Molecules: from Solid State to DNA and Drug Design, John Wiley & Sons, 2007.
[56] R.F. Bader, Atoms in Molecules, Wiley Online Library, 1990.
[57] I. Rozas, I. Alkorta, J. Elguero, Behavior of ylides containing N, O, and C atoms as hydrogen bond acceptors, J. Am. Chem. Soc. 122 (2000) 11154–11161.
[58] T.A. Keith, AIMAll (Version 15.09.27), T.K. Gristmill Software, Overland Park K.S., USA, 2016.
[59] E. Espinosa, E. Molins, C. Lecomte, Hydrogen bond strengths revealed by topological analyses of experimentally observed electron densities, Chem. Phys. Lett. 285 (1998) 170–173.
[60] P.W. Atkins, J. De Paula, Atkins' Physical Chemistry, 2010.
[61] C. Selvaraj, S.K. Singh, Validation of potential inhibitors for SrtA against Bacillus anthracis by combined approach of ligand-based and molecular dynamics simulation, J. Biomol. Struct. Dyn. 32 (8) (2014) 1333–1349.
[62] R.G. Parr, R.G. Pearson, Absolute hardness: companion parameter to absolute electronegativity, J. Am. Chem. Soc. 105 (1983) 7512–7516.
[63] A.K. Chandra, T. Uchimaru, Hardness profile: a critical study, J. Phys. Chem. A 105 (2001) 3578–3582.
[64] K. Mandal, T. Kar, P. Nandi, S. Bhattacharyya, Theoretical study of the nonlinear polarizabilities in H 2 N and NO 2 substituted chromophores containing two hetero aromatic rings, Chem. Phys. Lett. 376 (2003) 116–124.
[65] P. Nandi, K. Mandal, T. Kar, Effect of structural changes in sesquifulvalene on the intramolecular charge transfer and nonlinear polarizations–a theoretical study, Chem. Phys. Lett. 381 (2003) 230–238.
[66] P.K. Nandi, K. Mandal, T. Kar, Theoretical study of static second-order nonlinear optical properties of push–pull heteroquinonoid dimers, J. Mol. Struct. THEOCHEM 760 (2006) 235–244.
[67] H. Tanak, Density functional computational studies on 2-[(2, 4-Dimethylphenyl) iminomethyl]-3, 5-dimethoxyphenol, Int. J. Quantum Chem. 112 (2012) 2392–2402.
[68] C. Bosshard, J. Hulliger, M. Florsheimer, P. Gunter, Organic Nonlinear Optical Materials, CRC Press, 2001.
[69] C.-r. Zhang, H.-s. Chen, G.-h. Wang, Structure and properties of semiconductor microclusters Ga~ nP~ n (n= 1-4): a first principle study, Chem. Res. Chin. Univ. 20 (2004) 640–646.
[70] H.A. Kurtz, D.S. Dudis, Quantum mechanical methods for predicting nonlinear optical properties, Rev. Comput. Chem. 12 (1998) 241–280.
[71] A.K. Jeewandara, K.N. de Silva, Are donor–acceptor self organised aromatic systems NLO (non-linear optical) active? J. Mol. Struct. THEOCHEM 686 (2004) 131–136.
[72] A.D. Buckingham, Permanent and induced molecular moments and long-range intermolecular forces, Adv. Chem. Phys. Intermolecular Forces 12 (1967) 107–142.
[73] A. Hinchliffe, Ab initio studies of the dipole polarizabilities of conjugated molecules: Part 2. Monocyclic azines, J. Mol. Struct. THEOCHEM 304 (1994) 109–120.
[74] A. Hinchliffe, Ab initio studies of the dipole polarizabilities of conjugated molecules: Part 5. The five-membered heterocyclics C4H4E (E = BH, AlH, CH2, SiH2, NH, PH, O and S), J. Mol. Struct. THEOCHEM 331 (1995) 109–125.
[75] M. Toy, H. Tanak, DFT quantum chemical studies on 1-[n-(2-pyridyl) aminomethylidene]-2 (1h)-naphtalenone, J. Theor. Comput. Chem. 11 (2012) 745–762.
[76] H. Tanak, A.A. Ağar, O. Büyükgüngör, Experimental (XRD, FT-IR and UV–Vis) and theoretical modeling studies of Schiff base (E)-N′-((5-nitrothiophen-2-yl) methylene)-2-phenoxyaniline, Spectrochim. Acta Part A Mol. Biomol. Spectrosc. 118 (2014) 672–682.
[77] S. Kecel-Gunduz, S. Celik, A.E. Ozel, S. Akyuz, Structural and vibrational spectroscopic elucidation of sulpiride in solid state, J. Biomol. Struct. Dyn. 33 (2) (2015) 322–343.
[78] B. Kramer, M. Rarey, T. Lengauer, Evaluation of the FLEXX incremental construction algorithm for protein–ligand docking, Proteins Struct. Funct. Bioinform. 37 (1999) 228–241.